Earth and Planetary Science Letters 407 (2014) 109–122

Contents lists available at ScienceDirect

Earth and Planetary Science Letters

www.elsevier.com/locate/epsl

Variable crustal thickness beneath Thwaites Glacier revealed from airborne gravimetry, possible implications for geothermal heat flux in West Antarctica

Theresa M. Damiani [a,*], Tom A. Jordan [b], Fausto Ferraccioli [b], Duncan A. Young [c], Donald D. Blankenship [c]

[a] U.S. NOAA – National Geodetic Survey, 1315 East–West Highway, SSMC-3, N/NGS6 Room 8115, Silver Spring, MD 20910, USA
[b] British Antarctic Survey, High Cross, Madingley Road, Cambridge, CB3 0ET, UK
[c] Institute for Geophysics, Jackson School of Geosciences, University of Texas at Austin, J.J. Pickle Research Campus, Building 196, 10100 Burnet Road, Austin, TX 78758-4445, USA

ARTICLE INFO

Article history:
Received 18 November 2013
Received in revised form 12 September 2014
Accepted 16 September 2014
Available online 10 October 2014
Editor: P. Shearer

Keywords:
Thwaites Glacier
Marie Byrd Land
West Antarctic Rift System
crustal structure
airborne gravity
geothermal heat flux

ABSTRACT

Thwaites Glacier has one of the largest glacial catchments in West Antarctica. The future stability of Thwaites Glacier's catchment is of great concern, as this part of the West Antarctic Ice Sheet has recently been hypothesized to already be en route towards collapse. Although an oceanic trigger is thought to be responsible for current change at the grounding line of Thwaites Glacier, in order to determine the effects of this coastal change further in the interior of the West Antarctic Ice Sheet it is essential to also better constrain basal conditions that control the dynamics of fast glacial flow within the catchment itself. One major contributor to fast glacial flow is the presence of subglacial water, the production of which is a result of both glaciological shear heating and geothermal heat flux. The primary goal of our study is to investigate the crustal thickness beneath Thwaites Glacier, which is an important contributor to regional-scale geothermal heat flux patterns. Crustal structure is an indicator of past tectonic events and hence provides a geophysical proxy for the thermal status of the crust and mantle. Terrain-corrected Bouguer gravity disturbances are used here to estimate depths to the Moho and mid-crustal boundary. The thin continental crust we reveal beneath Thwaites Glacier supports the hypothesis that the West Antarctic Rift System underlies the region and is expressed topographically as the Byrd Subglacial Basin. This rifted crust is of similar thickness to that calculated from airborne gravity data beneath neighboring Pine Island Glacier, and is more extended than crust in the adjacent Siple Coast sector of the Ross Sea Embayment. A zone of thinner crust is also identified near the area's subaerial volcanoes lending support to a recent interpretation predicting that this part of Marie Byrd Land is a major volcanic dome, likely within the West Antarctic Rift System itself. Near-zero Bouguer gravity disturbances for the subglacial highlands and subaerial volcanoes indicate the absence of supporting crustal roots, suggesting either (1) thermal support from a warm lithosphere or alternatively, and arguably less likely; (2) flexural support of the topography by a cool and rigid lithosphere, or (3) Pratt-like compensation. Although forward modeling of gravity data is non-unique in respect to these alternative possibilities, we prefer the hypothesis that Marie Byrd Land volcanoes are thermally-supported by warmer upper mantle. The presence of such inferred warm upper mantle also suggests regionally elevated geothermal heat flux in this sector of the West Antarctic Rift System and consequently the potential for enhanced meltwater production beneath parts of Thwaites Glacier itself. Our new crustal thickness estimates and geothermal heat flux inferences in the Thwaites Glacier region are significant both for studies of the structure of the broader West Antarctic Rift System and for assessments of geological influences on West Antarctic Ice Sheet dynamics and glacial isostatic adjustment models.

Published by Elsevier B.V.

1. Introduction

Satellite observations (ERS-1, EnviSat, GRACE, and ICESat) over the last two decades have highlighted dynamic areas of the ice

* Corresponding author. Tel.: +1 240 997 1282; fax: +1 301 713 4327.
E-mail addresses: theresa.damiani@noaa.gov (T.M. Damiani), tomj@bas.co.uk (T.A. Jordan), ffe@bas.co.uk (F. Ferraccioli), blank@ig.utexas.edu (D.A. Young), duncan@ig.utexas.edu (D.D. Blankenship).
http://dx.doi.org/10.1016/j.epsl.2014.09.023
0012-821X/Published by Elsevier B.V.

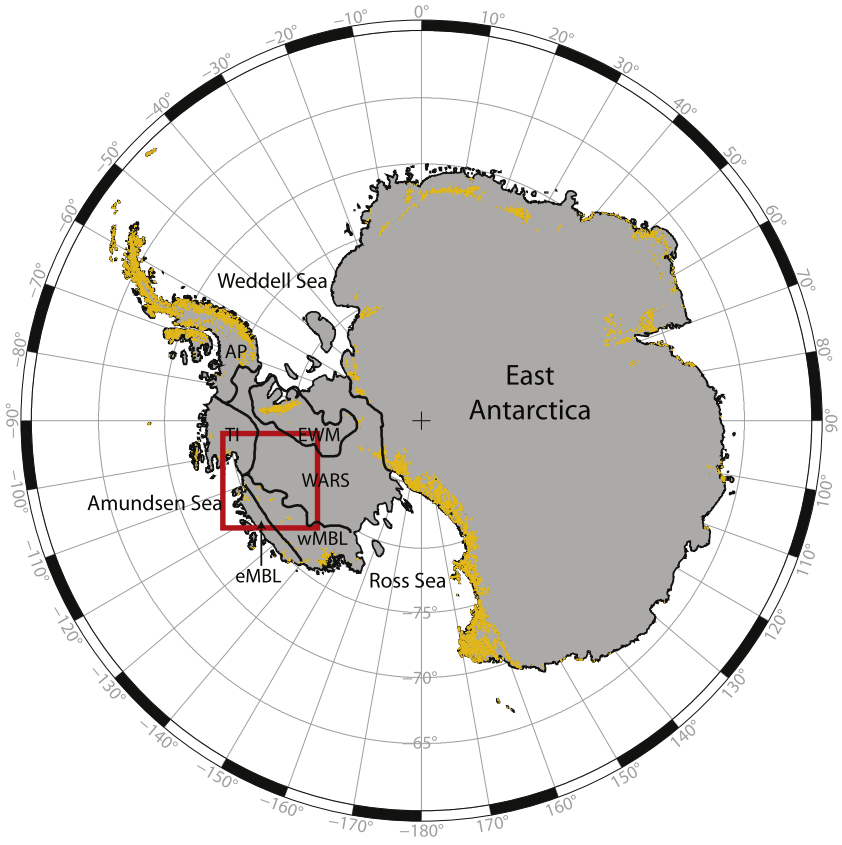

Fig. 1. Antarctic index map showing the location of all other figures for this paper (red box). Also shown: Antarctic coastline (SCAR, 2006) (thin black line), rock outcrop locations (gold lines) (SCAR, 2006) and previously-identified West Antarctic crustal blocks (thick back lines) (Dalziel and Elliot, 1982; Dalziel and Lawver, 2001). Crustal block names: AP = Antarctic Peninsula; TI = Thurston Island; EWM = Ellsworth–Whitmore Mountains; WARS = West Antarctic Rift System; eMBL and wMBL = eastern and western Marie Byrd Land. (For interpretation of the references to color in this figure legend, the reader is referred to the web version of this article.)

sheet. Among those is Thwaites Glacier (TG) in West Antarctica's Amundsen Sea Embayment (ASE, Figs. 1 and 2). Estimates of glacier mass loss, speed, and acceleration are dependent on the size of the catchment defined and the time period considered by each study, but are critical to understanding which parts of the ice sheet are changing. TG and neighboring Pine Island Glacier (PIG) are the fastest, most rapidly changing Antarctic glaciers and have the largest effect on ice sheet mass balance (Rignot et al., 2014). New and old studies agree with this assessment (Fahnestock and Bamber, 2001; Thomas et al., 2004; Rignot, 2006; Pritchard et al., 2009; King et al., 2012; Lee et al., 2012, Shepherd et al., 2012; Joughin et al., 2014; Rignot et al., 2014). Smaller glaciers to the west of TG (Haynes, Pope, Smith, Kohler) are often included in TG's catchment and are known to be thinning at high rates (Pritchard et al., 2009). TG and PIG are also vulnerable to ocean forcing at their grounding lines. They are minimally protected from encroaching warm ocean waters (Jacobs et al., 2012; Arneborg et al., 2012) by small, currently retreating, ice shelves (Alley, 2002; Vaughan et al., 2007; Pritchard et al., 2009; Rignot et al., 2013). Unequivocally, TG and its neighboring glaciers are a major source of ice loss for the West Antarctic Ice Sheet and experience rapid change.

Comparably little is known about the glaciers' subglacial environment. Geothermal heat flux (GHF) from the crust and mantle affect temperature in the overlying ice column and subglacial melt water production – two conditions that influence ice flow (Alley et al., 1986; Blankenship et al., 1986; Anandakrishnan et al., 1998; Bell et al., 1998; Blankenship et al., 2001; Studinger et al., 2001). In the last decade, basal water has been identified across the Ross Sea Embayment from: direct sampling of unfrozen, high water content tills at the bottom of boreholes (Kamb et al., 2001); analysis of airborne radar sounding basal reflections (Carter et al., 2007; Peters et al., 2007b); and seismic reflection amplitude versus offset analysis (Peters et al., 2007a). Also, ICESat satellite laser altimeter measurements have revealed an extensive network of subglacial lakes and active water movement between the lakes in the Ross Sea Embayment (e.g. Fricker et al., 2010). Subglacial water is now known to be widespread across the whole continent (Siegert et al., 2005; Fricker et al., 2010).

Evidence from TG basal shear stress models suggests widespread basal melting (Joughin et al., 2009). Also, subglacial water (from ocean incursions or from upstream sources) may play a controlling role in grounding line migration (Sergienko and Hindmarsh, 2013). Friction between the fast-moving ice and bedrock generates subglacial water beneath the glacier's trunk. Although basal melt rate calculations depend on accurately estimating the GHF in areas of slower-moving areas, a recent study assumed GHF under TG to be a constant 70 $mW\,m^{-2}$, meanwhile acknowledging that reported values for West Antarctica range between 50 $mW\,m^{-2}$ and 150 $mW\,m^{-2}$ (Joughin et al., 2009, references therein). A 10 $mW\,m^{-2}$ error in GHF corresponds to an ~10% change in basal melt rates calculations (Joughin et al., 2009), potentially leading to significant underestimation of basal melt rates if the subglacial GHF assumed is too low. The GHF used in the high resolution (Sergienko and Hindmarsh, 2013) inversion is not reported.

The uncertainty in GHF for West Antarctica remains large because direct measurements of heat flux are difficult to obtain. Additionally, there is much uncertainty about the history of mantle and crustal evolution in Antarctica, making theoretical estimation of GHF more difficult than for other continents. Thus, understanding the fast-flow of TG (and its neighboring glaciers) is reliant on

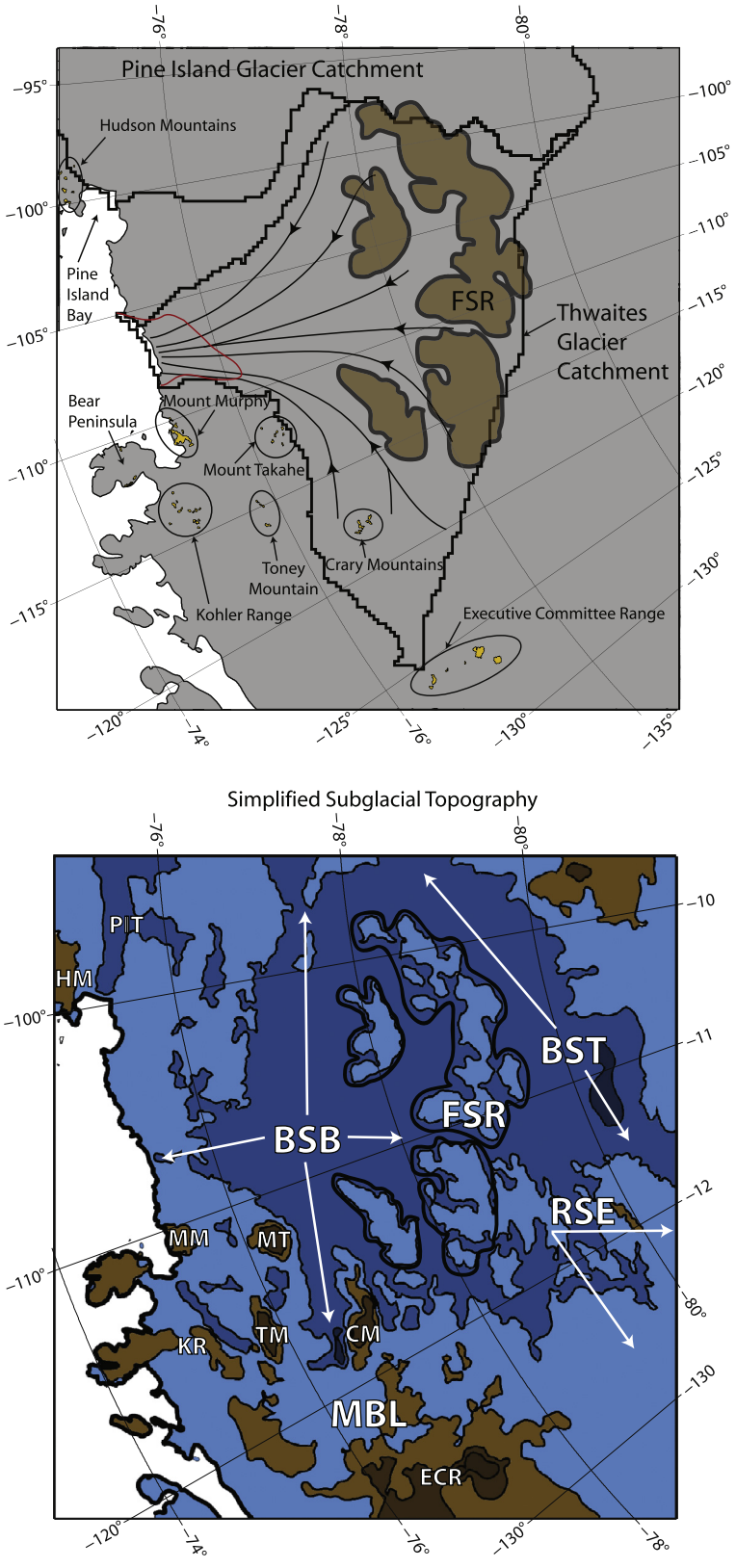

Fig. 2. Glaciological (top) and subglacial topographic (bottom) setting of the TG area. Top: Areas above sea level are colored gray. Rock outcrop locations (gold fill), major glacier catchments (thick black lines) (Vaughan et al., 1999), generalized ice flow lines for TG based on InSAR velocities (thin black lines, arrows indicate flow direction), and the area in which InSAR-measured ice flow velocities (Rignot, 2006) for TG exceed 500 m/yr (thin red line). The Former Sinuous Ridge (FSR) subglacial highlands are outlined in black and filled with brown. Circled and labeled areas are volcanic centers. Bottom: Subglacial bedrock topography in blue and subaerial in brown, simplified and colored by elevations: −2 km or deeper (dark blue), −1 to −2 km (royal blue), 0 to −1 km (light blue), 0 to 1 km (light brown), and 1 to 2 km (dark brown). Coastline (SCAR, 2006) shown in thick black. Major features: BSB = Byrd Subglacial Basin, FSR = Former Sinuous Ridge subglacial highlands (outlined in heavy black lines), BST = Bentley Subglacial Trench, RSE = Ross Sea Embayment, MBL = Marie Byrd Land. Other features: PIT = Pine Island Trench, HM = Hudson Mountains. Marie Byrd Land volcanoes: MM = Mount Murphy, MT = Mount Takahe, KR = Kohler Range, TM = Toney Mountain, CM = Crary Mountains, and ECR = Executive Committee Range. (For interpretation of the references to color in this figure legend, the reader is referred to the web version of this article.)

Table 1
Crustal thickness and Moho depths near the Byrd Subglacial Basin (BSB) and Marie Byrd Land (MBL).

Source	Measurement method/technique	Location	Crustal thickness or Moho depth?	Estimate (km)
Gohl et al. (2007)	Marine wide-angle refraction, magnetic, and gravity measurements	Inner continental shelf, North of MBL	Moho depth	23
		Inner continental shelf, North of BSB	Moho depth	25
Winberry and Anandakrishnan (2004)	Passive seismic data with receiver function analysis	Bentley Subglacial Trench (station MTM)	Crustal thickness	21
		Byrd Station, in the Ross Sea Embayment	Crustal thickness	27
		160 km SE of MBL	Crustal thickness	25
Luyendyk et al. (2003)	Bouguer gravity, modeled as terrain fully-compensated at Moho	Western MBL	Moho depth	28–31
		Ross Sea Embayment, Southwest of MBL	Moho depth	24–27
Ritzwoller et al. (2001)	Surface wave dispersion tomography	West Antarctica, Average of whole area	Crustal thickness	27
Bentley (1991)	Review paper, seismic (surface wave and refraction) and gravity measurements	West Antarctica, Range of values for "most places"	Crustal thickness	25–30
Jordan et al. (2010)	Airborne gravity modeling, pinned to a passive seismic site	Pine Island Glacier catchment, ~500 km West of MBL	Moho depth	18–20

understanding the composition, complexity, and history of the ASE crust and mantle. This study addresses the crustal context of TG by deriving new information on the crustal structure of the West Antarctic Rift System (WARS) and adjacent MBL volcanic dome by analyzing new airborne gravity data. The results of our study are important to geological studies of the WARS that rely on constraints on crustal structure to better comprehend the evolution of the rift system, and for glaciology, particularly for understanding the effects of GHF on subice hydrology and ice sheet dynamics, and also for glacial isostatic rebound estimations in West Antarctica.

1.1. Geologic and tectonic setting

Our knowledge of TG's ice-bed boundary comes from radar and free-air gravity studies of bed topography; basal shear stress estimates; and tectonic reconstructions. Radar-sounding (Holt et al., 2006) and free-air gravity (Diehl et al., 2008a; 2008b) studies revealed the morphology of the ice-bed interface across the catchment. The two tributaries on the eastern side of the catchment (nearer PIG, Fig. 2) flow through wide segments of the Byrd Subglacial Basin (BSB) that are >2 km below sea level and appear to be only weakly constrained by bedrock topography. The other (southern and western) tributaries exploit confined valleys in the former Sinuous Ridge and eastern MBL (Fig. 2). Together, the glacier's tributaries flow through a subglacial lowland that connects the TG and PIG catchments (via the BSB and Bentley Subglacial Trench, Fig. 2), and the Ross Sea Embayment (via the former Sinuous Ridge, Fig. 2) (Holt et al., 2006; Diehl et al., 2008b). The glacier's trunk flows south to north through the BSB (Fig. 2), which is 1–2.5 km below sea level.

The BSB's formation has been linked to the formation of the WARS (Dalziel and Lawver, 2001; Dalziel, 2006; LeMasurier, 2008; Figs. 1 and 2). The rift system's evolution began when an offshore spreading ridge was drawn into the West Antarctic margin's subduction zone around 115 Ma (Siddoway, 2008). Distributed extension and enhanced GHF in a broad back-arc region has been inferred in Cretaceous times (Siddoway, 2008) and lateral movement of discrete 'crustal blocks' has also been identified from paleomagnetic data as potentially affecting Thurston Island and MBL (Dalziel and Elliott, 1982; Dalziel and Lawver, 2001). The northeast limit of the Mesozoic/early Cenozoic rifting is in either the Amundsen Sea or Bellingshausen Sea (LeMasurier and Landis, 1997; LeMasurier, 2008; Bingham et al., 2012) and rifted crust has been imaged from airborne gravity data beneath PIG (Jordan et al., 2010). However, the crustal structure of the WARS has not been determined at regional-scale beneath TG prior to our study.

West Antarctic rifting is thought to have occurred in at least two major phases during the late Mesozoic and early Cenozoic, (Luyendyk et al., 2001; Eagles et al., 2004; Siddoway, 2008; Bingham et al., 2012). Specifically, argon–argon dating and apatite fission track dating of the rocks along older faults indicate continued heating until 101 Ma and two subsequent cooling (i.e. rifting) episodes: 97–88 Ma and 80–70 Ma in the MBL region (Siddoway, 2008). This two-stage cooling was also predicted by models of West Antarctic rifting process (Huerta and Harry, 2007). The subducted spreading ridge likely provided a continuous, source of enhanced mantle heat flux to the base of the West Antarctic crust that would however likely have decayed significantly into the early Cenozoic.

The MBL volcanic dome began uplifting much later, coincident with late Cenozoic (Neogene) WARS volcanism (LeMasurier and Landis, 1997). The uplift and volcanism could be from a mantle plume (LeMasurier and Landis, 1997). Visible evidence of localized Neogene and Quaternary (23 Ma to present) uplift and volcanism are: (1) the topographic MBL Dome (LeMasurier and Landis, 1997) roughly centered upon the suggested original crustal block (Fig. 1), and (2) localized volcanic outcrops on Neogene and Quaternary volcanoes (LeMasurier and Thompson, 1990; Fig. 2). Additionally, the very narrow and linear Pine Island Trough (located beneath PIG) could be a Cenozoic rift exploiting a Cretaceous block boundary (Jordan et al., 2010). The offshore Pine Island Bay troughs have been suggested as the MBL and the Thurston Island blocks crustal boundary (Gohl, 2012), implying that the boundary does not lie beneath TG.

1.2. Crustal structure

Crustal thickness is a useful proxy for rifting history. Crustal structure is reported as Moho depth or crustal thickness. Estimates of these near the TG catchment range from 21–31 km (Table 1; Luyendyk et al., 2003; Winberry and Anandakrishnan, 2004; Gohl et al., 2007; Ritzwoller et al., 2001; Bentley, 1991, Jordan et al., 2010). The largest estimates of MBL crustal thickness (Bentley, 1991; Luyendyk et al., 2003) are unreliable because the authors assumed that the topography was Airy isostatically compensated at the Moho, not allowing for thin crust to exist. Based on our own calculations (see the end of Section 3 for calculation description), 30–38 km thick crust would be needed to isostatically compensate MBL with Airy assumptions, which is thicker than all of the other crustal thickness estimates.

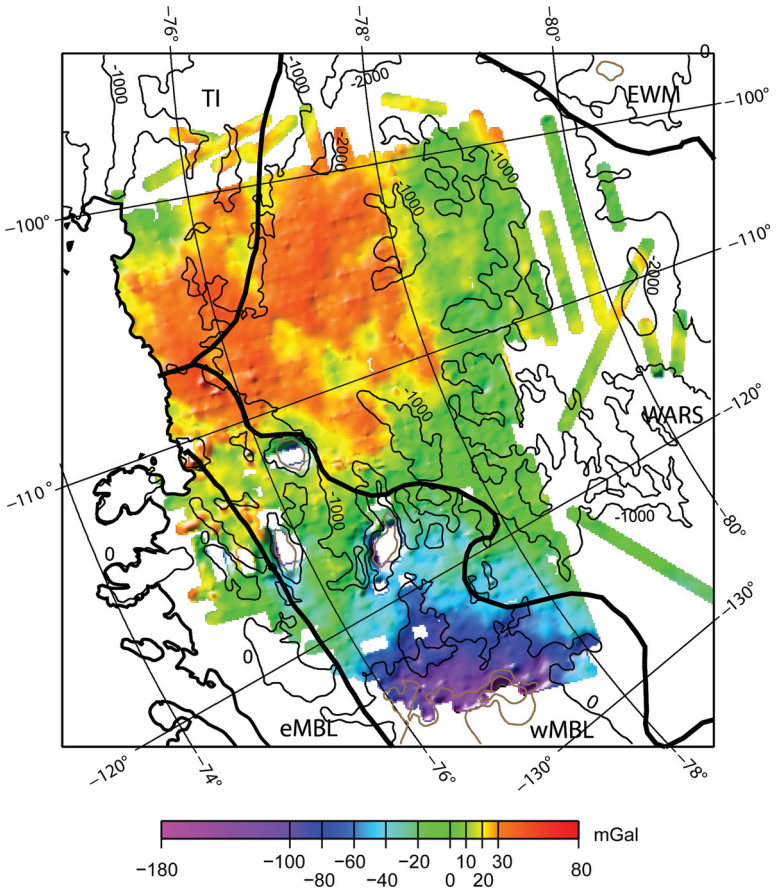

Fig. 3. Bouguer gravity disturbances for the AGASEA survey. Overlaid: 1000 m subglacial topographic contours (light black contours are at or below zero ellipsoidal height, coastline (SCAR, 2006) is medium weight black line, and brown contours above positive ellipsoidal heights). Heavy black lines = crustal blocks hypothesized by previous investigators (Dalziel and Elliot, 1982; Dalziel and Lawver, 2001); Block names: TI = Thurston Island; EWM = Ellsworth–Whitmore Mountains; eMBL and wMBL = eastern and western Marie Byrd Land; WARS = WARS.

If not Airy compensated, the crust is likely to be supporting the load (1) thermally, by a warm and buoyant mantle; (2) flexurally, by a cool and rigid lithosphere; or (3) with Pratt-like compensation due to laterally varying crustal density (LeMasurier and Landis, 1997; Winberry and Anandakrishnan, 2004). Two surface wave tomography studies that both imaged low-velocity mantle beneath MBL (Ritzwoller et al., 2001; Sieminski et al., 2003), support the thermal hypothesis. However, those studies are not conclusive either because the low velocity mantle could be caused either by temperature changes or chemical changes in the mantle.

2. Data

Airborne gravity data were collected by the University of Texas at Austin over TG in 2004–2005 (Diehl, 2008; Diehl et al., 2008a; Diehl et al., 2008b). A LaCoste & Romberg Air/Sea II gravimeter was installed in a DeHaviland Twin Otter as part of a multi-instrumented platform and final crossover analysis of the free-air gravity disturbances yielded a 2.3 mGal RMS error (Diehl et al., 2008b).

Interline and whole-survey bias problems are common in airborne gravity surveys. Biases arise from many sources, including errors in gravity ties, errors or simplifications in the GPS and gravity data processing, errors in the instrument calibration (Olesen, 2002), and/or errors in the correction for the sensor tilt (Olesen, 2002). Bias removal in airborne gravity data is still an active area of research, particularly in geodesy (e.g. Hwang et al., 2007). In geophysics, biases are often ignored because they do not impact interpretation of smaller-scale features. However, for crustal analyses the long-wavelength gravity field must be accurately determined. Here we use GRACE (Gravity Recovery and Climate Experiment) satellite gravity data to adjust the long-wavelength signal of the airborne gravity. Free-air gravity disturbances over Antarctica were calculated at the average AGASEA flight altitude from GGM03s model coefficients (Tapley et al., 2007), out to the same degree and order as the GGM03s model. A +9.7 mGal bias in the airborne gravity free-air disturbances was apparent compared to GRACE, so the published free-air gravity disturbances were adjusted. More complex methods of bias removal (e.g. Smith et al., 2013), nor the GOCE gravity model coefficients were available at the time of our analysis.

Terrain and bedrock heights above the WGS-84 ellipsoid used for the Bouguer correction (Fig. 2) are primarily from a grid of airborne ice-penetrating radar tracks with 15 km line spacing, which results in an ~9 km horizontal resolution; pre-gridding, the along-track sampling of the radar is one observation every ~17.7 meters (Holt et al., 2006; Vaughan et al., 2006). Ice sheet surface and subaerial volcano elevations come from a merged ICESat/ERS-1-derived digital elevation model (DEM) for West Antarctica (Bamber and Gomez-Dans, 2005).

3. Methods

Complete, terrain-corrected 3D Bouguer gravity disturbances (Fig. 3) were calculated to enhance the signals of crustal density anomalies, as free-air disturbances are dominated by the gravity effects of topography. Typical densities of ice and rock – 915 kg/m^3 and 2670 kg/m^3 respectively – were used. Ocean bathymetry just offshore of TG is poorly-constrained (Tinto and Bell, 2011), so a

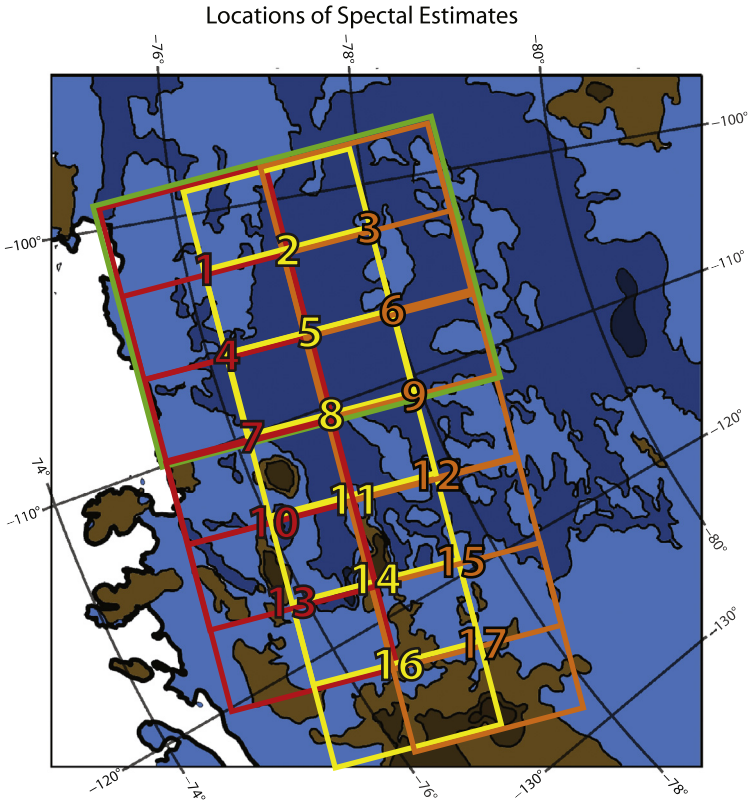

Fig. 4. Locations of the one 300 × 400 km (green) and seventeen 200 × 200 km radial power spectra estimates for gravity. Background image: Simplified subglacial topography, as shown in Fig. 2. Coastline (SCAR, 2006) shown in black, figure location with respect to Antarctica shown on Fig. 1. The location of the large estimate over the BSB is shown in green. Each small square (Supplementary Table 1) is numbered at its center and color-coded to match the label to the square: all squares along the coast are in red, those in the center of the area (the BSB and MBL) are in yellow, and those furthest into the interior (the Former Sinuous Ridge and MBL) are in orange. (For interpretation of the references to color in this figure legend, the reader is referred to the web version of this article.)

separate water correction was not included and Bouguer disturbances over floating ice were removed. The surface elevation DEM used in the Bouguer correction calculation underestimates the MBL volcano elevations (Young et al., 2008), thus disturbances over the volcanoes should be interpreted carefully.

The complete Bouguer correction was calculated by estimating the gravity effects of a slab plus regional topography on a spherical earth, in one step (von Frese et al., 1981). The gravity effect of input topography (or any discrete body) is calculated by approximating the body with gravitationally-equivalent point sources and then integrating over those point sources to get the total gravity effect at a given observation point. The integration is solved using Gauss–Legendre quadrature, leading to the moniker for the program, GLQ. The GLQ Fortran program assumes a constant density for the entire input body and a constant observation level above the body. For our data, the observation level was coincident with the maximum flight elevation (to which the data was upward continued prior to applying the Bouguer correction). Bodies above and below the datum (in our case, the ellipsoid) and bodies of different densities must each be treated separately by the GLQ program. So, the Bouguer calculation for the TG area was broken down into three calculations with different density contrasts: rock above the ellipsoid replacing air, ice above the ellipsoid replacing air, and ice below the ellipsoid replacing rock. Then, all three calculated gravity effects were combined into one Bouguer correction and applied to the free-air disturbances to yield the Bouguer disturbances.

Spectral analyses of gravity data provide estimates of the density structure of the crust (Spector and Grant, 1970; Karner and Watts, 1983; Fairhead and Okereke, 1988). This type of analysis has not been used often in recent decades because most areas of Earth have other geophysical datasets that can constrain gravity data models. However, the TG area is devoid of other published geophysical measurements (such as active seismic depths to the Moho). Power spectrum analysis is one of the very few methods with which to calculate crustal boundary depths solely from gravity.

A radial power spectrum is used to calculate the depth of interfaces because it is the average of all direction-dependent power spectra in the input data area, rendering the result independent of direction and easily visualized in 1-D. In other words, it is the ensemble power spectrum. The 1-D representation is plotted as the natural log of power versus wavenumber ($k = 1/(\text{wavelength})$). Piecewise linear regression yields a line slope (m) related to the depth (d) of each crustal density boundary, for example $d_{\text{Moho}} = 1/2m_{\text{MohoLine}}$ for the Moho density boundary between the crust and the mantle (Fairhead and Okereke, 1988). Spectral estimates should be done for areas of relatively homogeneous crustal structure so that slope breaks can be easily identified (Spector and Grant, 1970). Each slope break indicates that the spectrum's power above the break results from a different crustal density boundary than the power below the break.

Detailed variability in crustal structure is achieved by dividing the TG area into seventeen 200 × 200 km areas (Fig. 4) and examining both free-air and Bouguer gravity disturbances' radial power spectra. Mirroring each data area along two axes (N–S and E–W) improves recovery of long-wavelength signals (McNutt, 1983). For the 200 × 200 km squares, mirroring produces an 800 × 800 km area over which to calculate the power spectrum and allows depth estimates down to 67 km with <10% error (Regan and Hinze, 1976). The spectra for AGASEA data have a lower limit of useful information at the 9 km ($k = 0.1111$ km^{-1}) gravity data resolution and the upper limit of resolution is conservatively constrained by

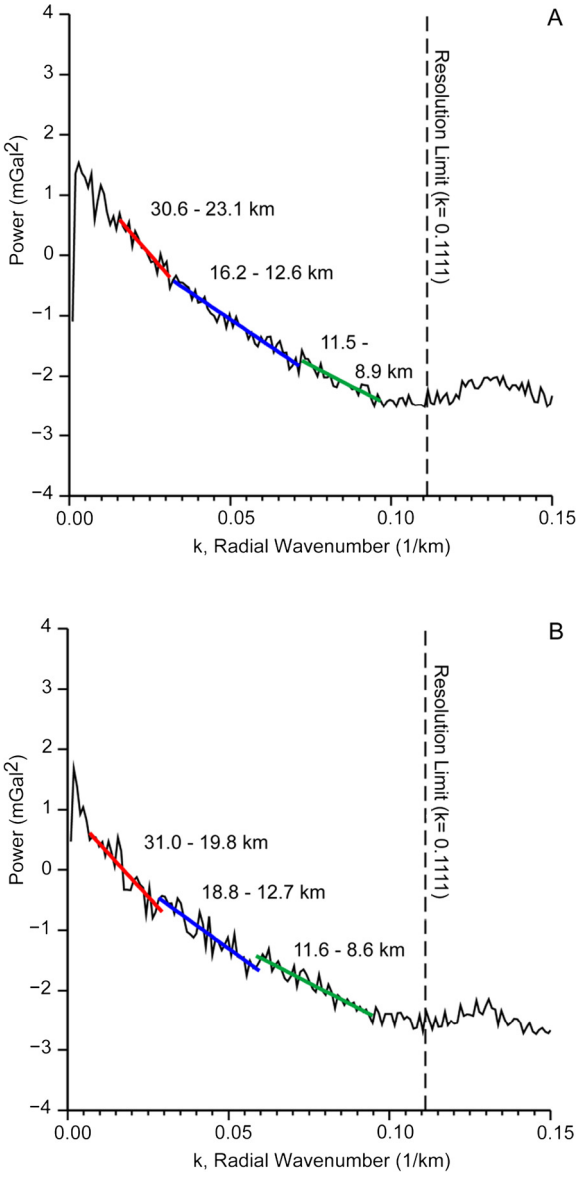

Fig. 5. Radial power spectra for the 400 × 300 km area within the BSB (BSB, green box on Fig. 4), A. Free-air gravity; B. Bouguer gravity. Line segments fit to find depths are colored and labeled with depth to boundary: Moho fit = red line; mid-crustal boundary 1 = blue line; and mid-crustal boundary 2 = green line (see text for description of boundaries). (For interpretation of the references to color in this figure legend, the reader is referred to the web version of this article.)

the size of the area ($k = 0.01$ km^{-1} for a 100 km maximum feature size; half of the original un-mirrored area's size). All radial power spectra were calculated using the open source code of the Generic Mapping Tools (GMT) by Wessel and Smith (1998).

Radial power spectra were fit with a series of least-squares, best-fit lines using GMT routines (Fig. 5). The end points of each line segment are chosen by eye at apparent slope breaks, identified visually by changes in the running slope of the line. After that, a linear regression is performed on that section of the power spectrum to ensure that the best-fit slope is obtained for that line segment. Regression error estimates given are 1-sigma numbers determined during regression. Since changes in the spectral slope can be subtle, plots of the spectral fits show the regression lines extended past the chosen break points (B, D; Figs. 6 and 7) to illustrate the piecewise nature of the spectral slopes.

The median depth value satisfying both spectral results is the final depth estimate for each boundary. Having both the free-air and Bouguer spectra allows: (1) two sets of related estimates for the depth of the crustal boundaries that are affected by some different error sources, which helps in verifying that a consistent slope break was chosen, and (2) an estimate of the errors affecting those two spectral estimates. The errors in the free-air disturbance spectra and Bouguer spectra are different, as is the strength of the crustal boundary signal in each spectrum.

For the spectral estimate of Moho depth to be biased by the gravity effects of large-scale, shallow-depth features – such as from volcanoes – those features would need to be associated with gravity signals of the same spatial wavelengths used to estimate crustal structure. As shown in Supplementary Table 1, the minimum and maximum wavelengths used to estimate the Moho depth were between 16 km and 100 km (equivalent to k values of 0.061 km^{-1} and 0.01 km^{-1}, respectively) and on average 23 km and 64 km (equivalent to k values of 0.043 km^{-1} and 0.016 km^{-1}, respectively).

The free-air disturbance, which includes more signal power from the volcanoes because of the contribution from their topography, would be most prone to this error. A cursory measurement of the spatial extent of the free-air gravity signals at the volcanoes and other subglacial topographic features shows power in wavelengths as long as 230 km, including in the range of the crustal depth estimate. However, the Bouguer gravity disturbance, which has been corrected for the shallow gravity sources of volcano topography, would have much less contribution to wavelengths in the 16 km to 100 km range used for crustal estimation. Visually, this can be seen in Fig. 3 as the broad Bouguer gravity features over volcanic areas. The Bouguer estimate will be more accurate in those areas, especially because of the excellent radar coverage of subglacial topography in the area. So, having two estimates allowed us to calculate an error based on the range of crustal depths that would satisfy both spectra, knowing that the free-air-derived estimate is more prone to error.

Data gaps in both the free-air and Bouguer disturbances were interpolated using a GMT tensioned spline prior to calculating the spectra, to avoid any spectral ringing from data line truncations. Even if the interpolation did not adequately represent features within the data gaps, the gaps are no larger than 60 km × 60 km in size (3600 km^2, only 10% of the un-mirrored block area), leaving 36 400 km^2 (90% of the un-mirrored block area) from which to calculate the power of shorter wavelength information.

The spectral analyses can constrain Bouguer gravity modeling, as done here with the GM-SYS iterative forward modeling package licensed through Geosoft's Oasis Montaj software, which is based on the classic multi-sided polygon modeling theories of Talwani et al. (1959). Three models (Fig. 6) were used to test crustal structure hypotheses: (1) crustal layers solely determined from spectral results; (2) crustal layers from spectral results plus any additional bodies required to test the thermally-supported MBL Dome hypothesis; and (3) crustal layers loosely guided within the error bounds of the spectral results to test the maximum possible crustal thickness beneath MBL. Densities were obtained from seismic profiles on the inner continental shelf in the ASE (Gohl et al., 2007) by converting P-wave velocities: 2600–2700 kg/m^3 (upper crust), 2800–2900 kg/m^3 (lower crust), and 3200–3300 kg/m^3 (upper mantle). The gravity forward models assume standard, constant layer densities. Because the modeling is non-unique, the models were kept as simple as possible for each hypothesis being tested.

Also, we calculated an "Airy Moho" to test whether the assumption of Airy isostasy (elastic thickness of the lithosphere equal to zero) was valid in the data area. The method we used, also employed by Jordan et al. (2010), condenses known non-rock surface loads into an effective topography. This is the usual first step toward calculating isostatic gravity disturbances (Jachens and Griscom, 1985). The condensation allows us to replace the mass

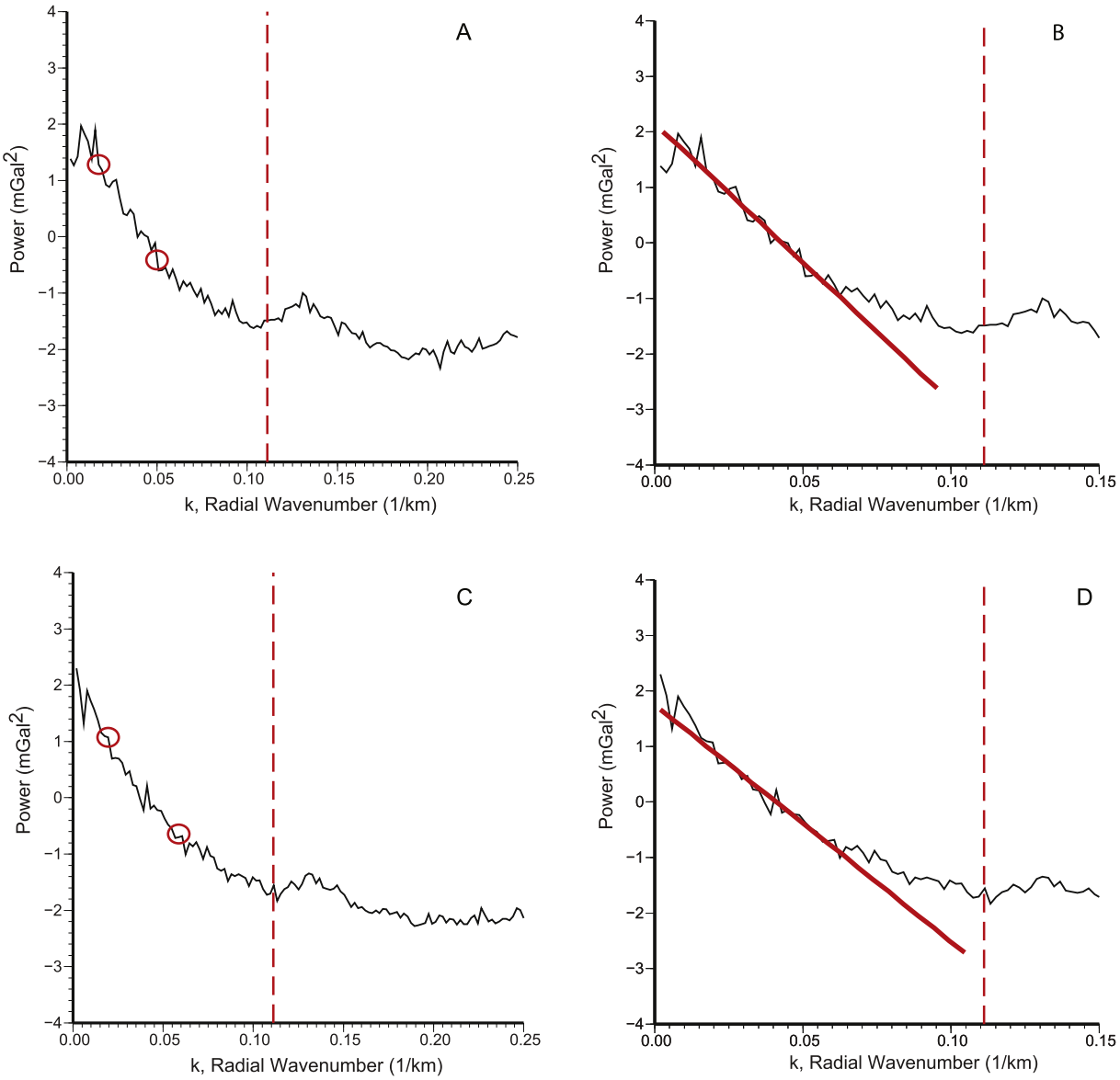

Fig. 6. Radial power spectra for a typical shallow crust 200×200 area. This example is Block 11, with a calculated Moho Depth of 19.3 ± 1.0 km. Free-air disturbance spectra with slope breaks marked (A, circles) and zoomed in with linear regression (B, heavy line), as well as the Bouguer disturbance spectra with slope breaks marked (C, circles) and zoomed in with linear regression (D, heavy line). The vertical dashed line is the resolution limit of the data ($k = 0.1111$).

of the ice with a gravitationally-equivalent mass of rock. The subglacial topography, plus the condensed ice, act as the surface load. Compensation of that load is assumed to happen at the Moho, as dictated by Airy isostasy. The calculation of the undulations in the Airy Moho is done with the GMT grdfft command. The resulting Airy Moho undulations must be pinned to an absolute *a priori* Moho depth, here a seismic receiver function estimate of 28 km crustal depth at Byrd Station (Winberry and Anandakrishnan, 2004). When comparing the seismically-pinned Airy Moho to the Moho calculated by the gravity spectral method, if the two match (to within error) then the topographic load is considered Airy compensated; if the gravity-derived Moho is shallower then the load is undercompensated; and if the gravity-derived Moho is deeper then the topographic load is overcompensated (Fig. 9).

4. Results

Fig. 3 shows a regional positive Bouguer disturbance (~40 mGal) that coincides with the BSB beneath TG, as well as with Mt. Murphy and the Kohler Range. Surrounding that is a zone of near zero-magnitude Bouguer disturbances. A regional negative Bouguer disturbance west of the Crary Mountains reaches −180 mGal over the Executive Committee Range. This regional negative disturbance may be even more negative than the values we report here because of the DEM height inaccuracies mentioned above.

Spectral analyses of a 400×300 km area within the BSB (Fig. 4, green box) had subtle changes in slope (Fig. 5), signifying large changes in crustal boundaries within the basin. The best-fit Moho and mid-crust boundary depths are 26.85 ± 3.75 km and 12.55 ± 3.65 from free-air gravity and 25.4 ± 5.6 km and 13.7 ± 5.1 km from Bouguer gravity, respectively. The error bars on the depth estimates are large, underscoring that the depths to these boundaries vary across the area. More detailed spectral results from the seventeen 200×200 km areas are presented in Fig. 9 and Supplementary Table 1. These smaller areas show shallow Moho depths and under-compensated crust in the interior of the catchment, with increasing Moho depth and compensation towards the coast. The Moho depths across all areas range from 30.6 to 18.6 km. The

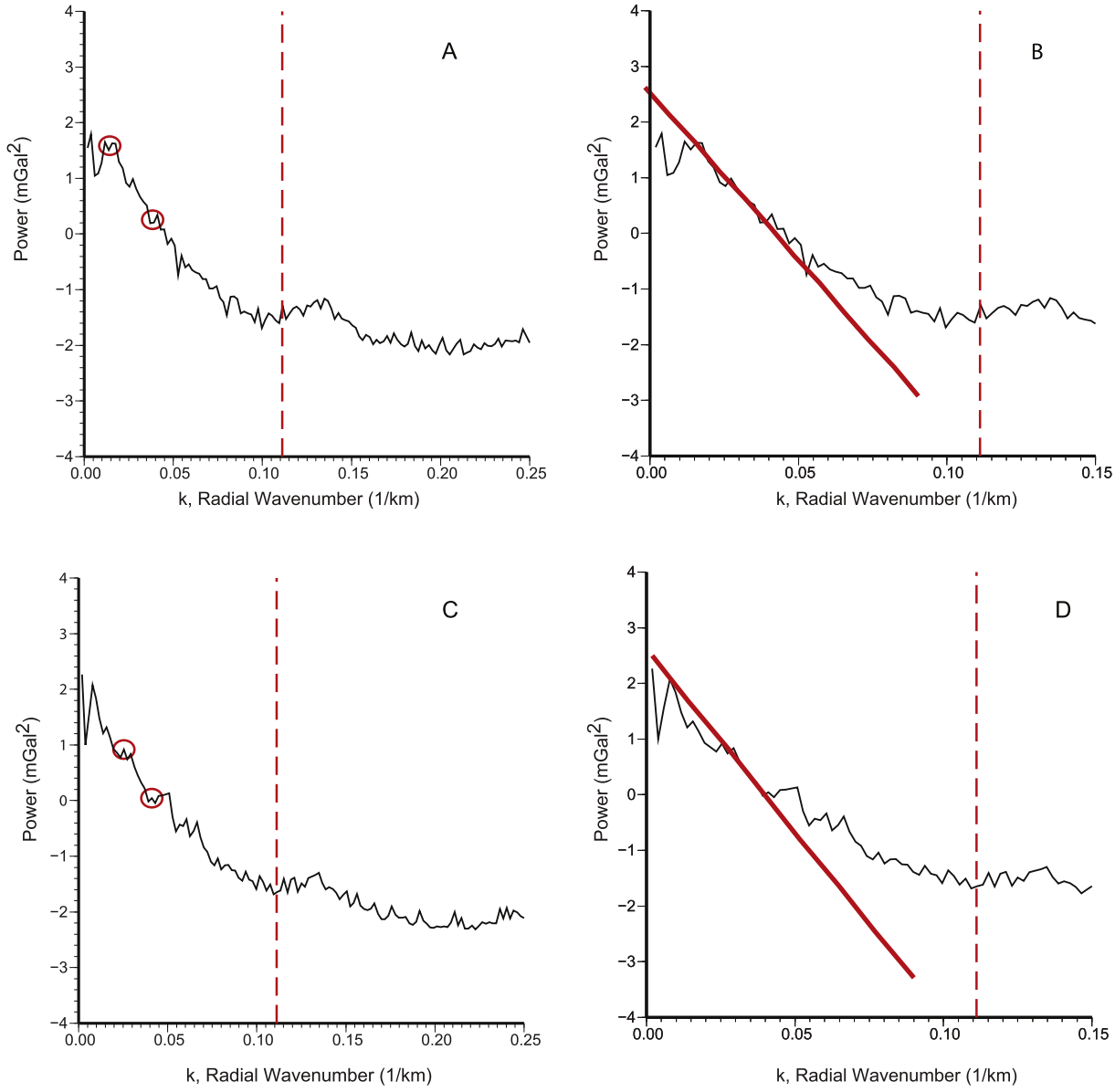

Fig. 7. Radial power spectra for a typical deeper crust 200 × 200 area. This example is Block 13, with a calculated Moho Depth of 28.4 ± 1.3 km. Free-air disturbance spectra with slope breaks marked (A, circles) and zoomed in with linear regression (B, heavy line), as well as the Bouguer disturbance spectra with slope breaks marked (C, circles) and zoomed in with linear regression (D, heavy line).

average Moho depth over the broad BSB from the 200 × 200 km areas is 24.7 km, which is similar to the 400 × 300 km whole-area BSB estimates. The deepest, ~30 km Moho depth areas are not continuous, but are separated by pieces of relatively thinner crust. The thinnest crust occurs at the Crary Mountains.

Out of three forward models attempted (Fig. 8), only the second two fit the observed regional gravity trends. The first model's strict interpretation of the spectral boundary depths cannot reproduce the trends of the observed gravity, which is not surprising as spectral estimates only capture broad crustal structure and not smaller structures or density differences that would be resolved on a more detailed modeling profile. The second model, which attempts to capture heterogeneity within the crust and mantle, adds a lower-density upper mantle body (100 kg/m^3 less than surrounding mantle) beneath MBL. If the body lies adjacent to the lower crust, then it extends down to 42 km depth to fit the observed gravity and there must be a large body of higher-density crustal material in the adjacent rift area (Fig. 7). A less extreme mantle density contrast would imply significantly thicker low density mantle beneath MBL, which would be consistent with a mantle plume hypothesis (LeMasurier and Landis, 1997). The third model uses the spectral depths only as a rough guide, and tests how thick the crust beneath MBL could be. Though non-unique, this model obtains a good gravity fit for BSB rift Moho depths of 18–19 km and MBL depths from 20 km to 25 km, deepening westward (Fig. 8).

5. Crustal structure discussion

The pattern of Bouguer gravity disturbances reveals laterally-variable crust and mantle beneath TG and MBL (Fig. 3) and variable spectral Moho depth estimates that are relatively shallow throughout (Fig. 9; Supplementary Table 1). The shallow Moho (19–24 km deep) discovered here beneath TG's broad BSB lends support to the hypothesis that this region was affected by distributed Cretaceous rifting. Thus, the undeformed Thurston Island crustal block does not extend into the area beneath the glacier and the glacier does not flow along a boundary between the crustal blocks as previously hypothesized (Dalziel and Lawver, 2001). There is a single

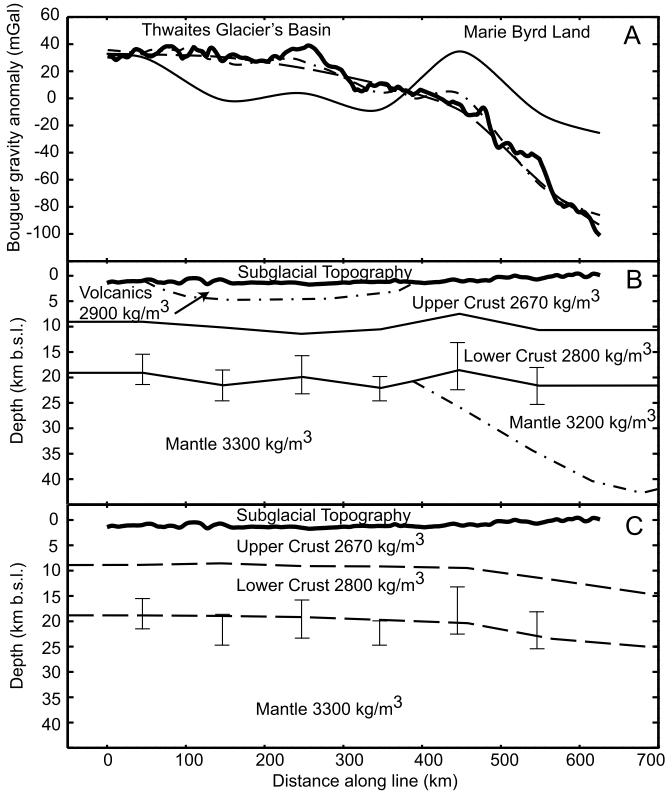

Fig. 8. A: Fit of Bouguer gravity calculated for 3 different models to the Bouguer gravity calculated from the measured data (heavy solid line). B and C: Three crustal models. Crustal model 1 (panel B) is represented with solid lines and is constrained solely by spectrally-defined boundary depths. Crustal model 2 (panel B) is crustal model 1 plus the addition of the dash-dot lines indicating inferred density differences needed to fit the Bouguer gravity calculated from the measured data. Crustal model 3 is constrained loosely (within the error bounds) to the spectrally-defined boundary depths. Radar-measured subglacial topography is on panels B and C (heavy black line). On all models, subglacial topography is shown only for reference and was not included in the modeling. Model residual statistics are included in Supplementary Table 2. Profile location shown in red on Fig. 9.

spectral estimate of deeper crust (Block #1, Fig. 9) in the region of the hypothesized Thurston Island block, but a neighboring geophysical survey over PIG (Jordan et al., 2010) showed no evidence of a crustal block continuing from that corner (Block #1) to beneath the mouth of PIG. Thus, it seems unlikely that the small extent beneath the spectral depth estimate (Block #1) is a major crustal block.

The Bouguer disturbances confirm that the WARS continues into the western part of the neighboring PIG catchment, as recognized by Jordan et al. (2010). Our estimates of Moho depths there are shallower than the ~27–28 km estimated by others for the Ross Sea Embayment (Clarke et al., 1997; Winberry and Anandakrishnan, 2004). The shallower Moho implies either more intense Cretaceous rifting, thinner crust before initiation of Cretaceous rifting, or significant additional Cenozoic extension not seen in the Siple Coast sector of the Ross Sea Embayment. Although gravity results alone cannot differentiate between these three possibilities, LeMasurier (2008) hypothesized that the entire BSB region was affected by more widespread Neogene extension and Bingham et al. (2012) also discussed the possibility of Cenozoic extension affecting a larger sector of the WARS.

The shallowest (18–20 km) spectral Moho depths are recovered over the BSB, the former Sinuous Ridge, and the non-Executive Committee Range MBL volcanoes. Forward modeling (Fig. 7) suggests that the BSB may have been intruded by higher-density igneous rock in the upper crust. This interpretation is strongly supported by independent studies of aeromagnetic data over the region that suggest a highly magmatic segment of the rift that was affected by voluminous Cenozoic magmatism (Ferraccioli et al., 2007; Bingham et al., 2012).

A new boundary between the WARS and the MBL Dome is proposed based on the spectral crustal thickness results. The proposed boundary occurs within a zone around the two shallowest Moho depths (squares #14 and #15, Figs. 4 and 9) and the 20.5 km Moho depth (square #10, Figs. 4 and 9) between Mount Takahe and Toney Mountain. The thin crust there appears to have been exploited by the MBL subaerial volcanoes and suggests that late Cenozoic activity may focus around reactivated Cretaceous and or early Cenozoic rift-related structures. By inference, the most southern piece of thin crust (square #15, Figs. 4 and 9), which does not have subaerial volcanoes, has a high likelihood of containing recently active subglacial volcanoes.

Within MBL, forward modeling results show that the regional negative Bouguer disturbance can be interpreted as either thicker crust or thin rifted crust underlain by a low-density upper mantle body (Fig. 8, statistics in Supplementary Table 2). The 21.6–22.2 km spectrally-defined Moho depths suggest thinner crust than the 23–25 km crustal thicknesses from seismic results nearest MBL (Table 1, Fig. 9). The forward gravity model that estimates the maximum depth of the MBL Moho also indicates relatively thin crust (Fig. 8), comparable to the maximum seismic results in the region. The relatively uniform crustal thickness between the center of TG and MBL demonstrates that the elevated topography in MBL is not Airy isostatically-compensated. Lithospheric flexural support of high topography over a large area of thin crust is unlikely. Overall, the analyses presented here support the hypothesis of a thermally-supported crust in MBL, but are not conclusive due to the limitations of gravity-only analyses in resolving density vs. depth relationships.

In contrast to MBL, the zone of undercompensated topography (Moho depths that are 4.1 km to 6.5 km shallower than predicted by Airy isostasy) around the former Sinuous Ridge and adjacent to the BSB suggests flexural or Pratt-like support of the subglacial highlands. Speculatively, the former Sinuous Ridge could be composed of volcanic constructs emplaced in the Cenozoic upon the thin but cooled (and therefore more rigid) Cretaceous rift system lithosphere. Prominent magnetic anomalies in a small section of the highlands have been identified as subglacial volcanics (Jankowski and Drewry, 1981; Behrendt et al., 2004) and these anomalies are now much more clearly identified in new aeromagnetic data over the region (Ferraccioli et al., 2007).

6. Inferences for subglacial GHF

Based on a global data set of modern heat flow measurements, the global average continental heat flux is 65 ± 1.6 mW m^{-2}, with significant variations in flux depending on the basement rock type and age (Pollack et al., 1993). Older sections of the WARS would likely have bedrock formed of either: (a) Mesozoic igneous rocks, (b) Mesozoic or Cenozoic sedimentary rocks or (c) Mesozoic and older Paleozoic metamorphic rocks, which would typically have GHFes of 64.2 ± 28.8 mW m^{-2}, 63.7 ± 28.2 mW m^{-2}, or 63.9 ± 27.7 mW m^{-2}, respectively (Pollack et al., 1993). Error is expressed as one standard deviation. Areas that have experienced widespread Cenozoic igneous activity typically have a higher average heat flux of 97.0 ± 66.9 mW m^{-2} (Pollack et al., 1993). The standard deviation on the reported global average heat fluxes are large, but the numbers for the older rift indicate that it would be statistically unlikely to observe a heat flux higher than 93.0 mW m^{-2}, and unprecedented above 97.0 mW m^{-2}, in areas affected by only Mesozoic rifting and/or by Mesozoic and younger metamorphism and sedimentation. High heat fluxes in West Antarctica would be strongly indicative of Cenozoic magmatic activity. Thus, measure-

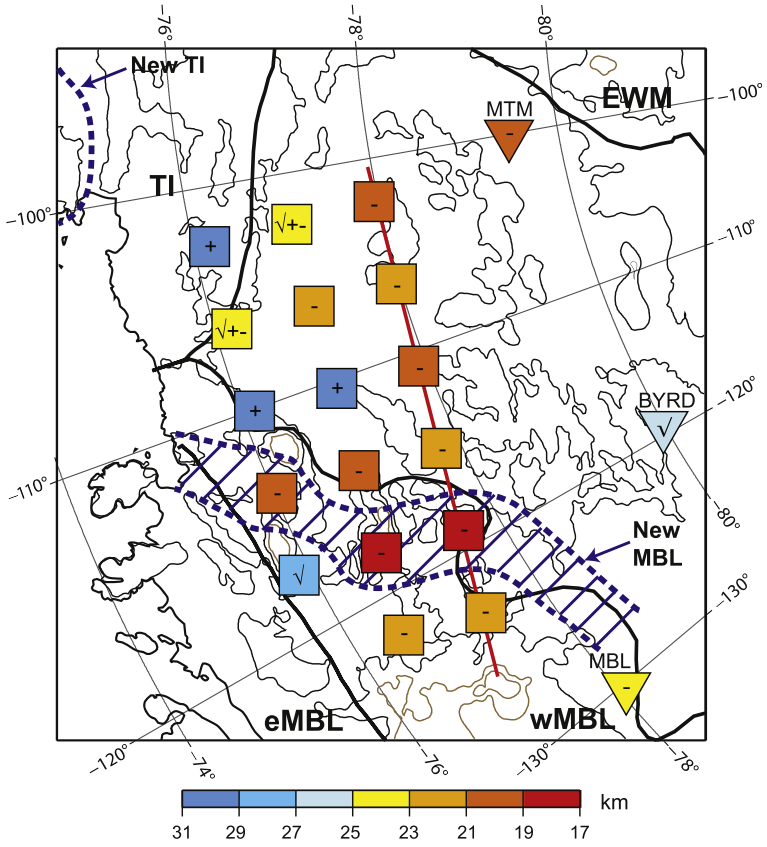

Fig. 9. Spectrally-defined Moho depth estimates (Supplementary Table 1) centered on the squares over which they were calculated (Fig. 4). Inverted triangles are Moho depths from Winberry and Anandakrishnan (2004), labeled with their station names. Checkmarks indicate Airy isostatic equilibrium, while pluses and minuses indicate over- or under-compensation of topography respectively. Red line = forward models' (Fig. 8) location. Blue dotted lines = revised crustal boundary locations based on these results. Background: Subglacial topography contours as in Fig. 3. Heavy black lines = crustal blocks (Dalziel and Elliot, 1982; Dalziel and Lawver, 2001): TI = Thurston Island; EWM = Ellsworth–Whitmore Mountains; eMBL and wMBL = eastern and western Marie Byrd Land. (For interpretation of the references to color in this figure legend, the reader is referred to the web version of this article.)

ments of GHF within the rift system could be used to infer the rift's history and current state of activity.

Thick ice cover over most of the continent makes GHF measurements difficult in Antarctica. Two exist in West Antarctica. At the bottom of the Siple Dome ice core borehole GHF is 69 $mW\,m^{-2}$ (Engelhardt, 2004), close to continental average. Siple Dome is located far from known areas of volcanic activity in the Ross Sea Embayment. However, very high GHF was reported from more recent drilling at WAISCORE (up to 200 $mW\,m^{-2}$) by Clow et al. (2012).

Other proxy measurements have been used to examine West Antarctic heat flux patterns, with varying results. A minimum average geothermal flux of 114 ± 10 mW/m has been inferred from an analysis of airborne radar-derived estimates of basal melting patterns beneath TG, with areas of higher flux exceeding 200 mW/m^2 (Shroeder et al., 2014), consistent with hypothesized rift-related Cenozoic magmatism in the region (Ferraccioli et al., 2007; Bingham et al., 2012; Behrendt et al., 2013). Seismic tomography results indicate normal velocity mantle in the Ross Sea Embayment, which can be interpreted as cooled mantle, but relatively slower velocity mantle in the ASE and MBL, which can be interpreted as warmer mantle (Ritzwoller and Shapiro, 2003; Sieminski et al., 2003). Magnetotelluric measurements found high resistivity at mantle depths in the Ross Sea Embayment interpreted as possibly indicating cooled mantle (Wannamaker et al., 1996). Satellite magnetic data modeling estimated 60 ± 25 $mW\,m^{-2}$ to 70 ± 25 $mW\,m^{-2}$ heat flux in the center of the West Antarctic Rift but much higher heat flux (upwards of 100 ± 25 $mW\,m^{-2}$) in the Ross Sea Embayment and MBL (Fox Maule et al., 2005). Topographical comparisons of the rift basin's depth in the Ross Sea Embayment and ASE suggest long-term cooling has already occurred (LeMasurier, 2008). There are therefore two seeming contradictory lines of evidence for GHF in both the Ross and ASE sectors of the WARS from satellite magnetic modeling and seismic tomography (Fox Maule et al., 2005; Shapiro and Ritzwoller, 2004). These inconsistencies are likely to reflect the paucity of local seismological observations over the region (that are required to better constrain both crustal and lithospheric structure) and the greater sensitivity to intra-crustal sources of GHF intrinsic in satellite-derived magnetic studies of GHF.

Beneath MBL and the Ross Sea, however, the lithosphere appears to be relatively warmer. Evidence shows localized, hot, volcanically-active areas that have either persisted into or restarted in the Neogene and Quaternary (<23 Ma). In addition to suggestions of warmer mantle there from the global studies mentioned above, it is well-known that Mt. Erebus on Ross Island is presently active and the other volcanoes on the island have been active in the recent past (LeMasurier and Thompson, 1990). Heat flux on Ross Island (near McMurdo Station) is 164 ± 60 $mW\,m^{-2}$ (Risk and Hochstein, 1974), which is considered very high. A subglacial volcano in the Ross Sea Embayment known as Mt. Casertz has shown evidence of recent activity on radar sounding records (Blankenship et al., 1993; Vogel and Tulaczyk, 2006). Subaerial volcanoes of Neogene and Quaternary ages also dominate MBL and the western edge of the ASE (LeMasurier and Thompson, 1990). In the TG catchment area, six subaerial volcanic centers (Figs. 1 and 2) have been active since the Neogene (LeMasurier and Thompson, 1990). The youngest subaerial volcano in the TG area, Mt. Takahe, has

been active over the last 40 000 years, as shown from ash layers found in the Byrd ice core that are geochemically identical to Mt. Takahe rock samples (Palais et al., 1988). The Hudson Mountains subglacial volcano that is very near the mouth of PIG is also considered to be recently active (Corr and Vaughan, 2008).

All of these studies suggest that focused areas of higher than average GHF have existed through the late Cenozoic, including the Quaternary, in MBL. If the GHF proxies are correct, we would expect West Antarctica to have a geographically-dependent mixture of both average and much higher than average heat flux, depending on their crustal setting with respect to the WARS and the MBL Dome.

6.1. This study's inferred GHF

Based on our new crustal structure calculations and previous tectonothermal work done in West Antarctica, we would expect significantly higher subglacial heat fluxes in the MBL area and an abundance of subglacial melt water to be available for TG's fast flow, as well as for Thwaites' western neighboring glaciers. Interestingly, the western side of TG, fed by tributaries originating in MBL, flows faster than the eastern side of the glacier. This could be an indication of water being fed into that side of the glacier from the MBL Dome area.

For GHF, we suggest that West Antarctic studies of areas with evidence for both Mesozoic rifting and late Cenozoic activity (such as for TG) a GHF estimate of at least 97 $mW\,m^{-2}$ is appropriate. This is the global average for areas of Cenozoic volcanic activity (Pollack et al., 1993). However, the spatial variability in crustal structure and in heat flux estimates in West Antarctica as a whole indicate, unsurprisingly, that any single GHF number is inadequate to describe the complexity of such a large area (e.g. Davies, 2013).

As with any parameter that has a high value of uncertainty and/or spatial variability, we recommend that studies using GHF values include sensitivity analyses in their research to explore the impact of different heat flux values on their models, as Joughin et al. (2009) did for their basal shear stress estimates. As mentioned in Section 1, they assumed 70 $mW\,m^{-2}$ GHF. That estimate is 27 $mW\,m^{-2}$ lower than our suggested value. However, because they performed a sensitivity analysis, we know that a 10 $mW\,m^{-2}$ error in GHF corresponds to an ~10% change in basal melt rates calculations (Joughin et al., 2009). Using our suggested higher number, basal melt rates at TG could be ~27% higher than the already widespread basal melting reported by Joughin et al.

7. Conclusions

The Bouguer gravity disturbances over TG from airborne surveying have provided a critical source of information for understanding the glacier's crustal context. The deep, broad BSB through which the glacier flows is part of the WARS that was likely affected by at least two stages of rifting in Cretaceous and Cenozoic times. The Bouguer gravity disturbances show clearly that the unrifted Thurston Island crustal block does not extend beneath TG, signaling that a redefinition of the crustal block boundaries in the ASE is needed. The deep topography of the BSB is underlain by highly thinned continental crust. The deepest confined troughs between the former Sinuous Ridge highlands are likely to be a result of glacial erosion. However, the deepest parts of the BSB likely reflect glacial overdeepening of the WARS as hypothesized for PIG (Jordan et al., 2010) and the Ferrigno Rift (Bingham et al., 2012) in the Bellingshausen Sea Embayment.

The MBL-BSB boundary is redefined (Fig. 9) as a zone of the thinnest crust (18 km Moho depths) yet found outside the Ross Sea. The zone occurs within the eastern MBL volcanoes, suggesting volcanic exploitation of a pre-existing crustal boundary. MBL crust is slightly thicker (~24 km Moho depth) than that observed in the BSB but thinner than surrounding seismic estimates and much thinner than predicted by Airy isostatic compensation. The regional negative Bouguer disturbance in MBL is adequately explained by low-density upper mantle beneath MBL. These results are consistent with the geophysical and geologic studies done to date in MBL and support the hypothesis that MBL has thin crust, and is thermally-supported by warm mantle. We suggest that a GHF number closer to 97 $mW\,m^{-2}$ is more appropriate for the area near TG, though that number is likely to be spatially-variable.

The results of this study will be of use for other research done in Antarctica. Glacial isostatic rebound modelers should use shallower Moho depth estimates for the ASE sector and more rigid, cooled lithosphere elsewhere, except in MBL where thin crust is likely to be hot and weak. Seismic topography models that prescribe crustal thickness should use thinner but heterogeneous WARS crust (thicker in the Ellsworth–Whitmore Mountains and thinner both in the MBL Dome and the WARS). Studies that utilize a GHF term, including basal melt calculations, should not assume continental average GHF in areas with thin crust and a recent history of volcanism, particularly MBL and probably the BSB as well. If MBL has been volcanically and also tectonically-active in the Quaternary and in Neogene times, as its tectonic history and our study suggest, then geothermal flux could have values up to 200 mW/m^2 (Clow et al., 2012; Schroeder et al., 2014). It is also clear that crustal block locations in West Antarctica must be re-defined, especially for the Thurston Island and MBL blocks.

Acknowledgements

This work was supported by the National Science Foundation (grants OPP-0230197 and ANT-0636724), the University of Texas Geology Foundation and Jackson School of Geosciences, the G. Unger Vetlesen Foundation, the University of Texas Institute for Geophysics Gale White Fellowship, the British Antarctic Survey, and NOAA's National Geodetic Survey. I would like to thank Vicki Childers, Jack Holt, and Scott Kempf for their assistance with this work.

Appendix A. Supplementary material

Supplementary material related to this article can be found online at http://dx.doi.org/10.1016/j.epsl.2014.09.023.

References

Alley, R.B., 2002. On thickening ice? Science 295, 451–452.
Alley, R.B., Blankenship, D.D., Bentley, C.R., Rooney, S.T., 1986. Deformation of till beneath ice stream-B, West Antarctica. Nature 322, 57–59.
Anandakrishnan, S., Blankenship, D.D., Alley, R.B., Stoffa, P.L., 1998. Influence of subglacial geology on the position of a West Antarctic ice stream from seismic observations. Nature 394, 62–65.
Arneborg, L., Wahlin, A.K., Bjork, G., Liljebladh, B., Orsi, A.H., 2012. Persistent inflow of warm water onto the central Amundsen shelf. Nat. Geosci. 5, 876–880. http://dx.doi.org/10.1038/ngeo1644.
Bamber, J., Gomez-Dans, J.L., 2005. The accuracy of digital elevation models of the Antarctic continent. Earth Planet. Sci. Lett. 237. http://dx.doi.org/10.1016/j.epsl.2005.06.008.
Behrendt, J.C., Blankenship, D.D., Morse, D.L., Bell, R.E., 2004. Shallow-source aeromagnetic anomalies observed over the West Antarctic ice sheet compared with coincident bed topography from radar ice sounding—new evidence for glacial "removal" of subglacially erupted late Cenozoic rift-related volcanic edifices. Glob. Planet. Change 42, 177–193.
Behrendt, J.C., Lemasurier, W.E., Cooper, A.K., Tessensohn, F., Trehu, A., Damaske, D., 2013. The West Antarctic Rift System: a review of geophysical investigations. In: Contributions to Antarctic Research II. American Geophysical Union, pp. 67–112.
Bell, R.E., Blankenship, D.D., Finn, C.A., Morse, D.L., Scambos, T.A., Brozena, J.M., Hodge, S.M., 1998. Influence of subglacial geology on the onset of a West Antarctic ice stream from aerogeophysical observations. Nature 394, 58–62.

Bentley, C.R., 1991. Configuration and structure of the subglacial crust. In: Tingey, R.J. (Ed.), The Geology of Antarctica. In: Oxford Monographs on Geology and Geophysics. Oxford University Press, Oxford, UK, pp. 335–364.

Bingham, R.G., Ferraccioli, F., King, E.C., Larter, R.D., Pritchard, H.D., Smith, A.M., Vaughan, D.G., 2012. Inland thinning of West Antarctic Ice Sheet steered along subglacial rifts. Nature 487, 468–471. http://dx.doi.org/10.1038/nature11292.

Blankenship, D.D., Bell, R.E., Hodge, S.M., Brozena, J.M., Behrendt, J.C., Finn, C.A., 1993. Active volcanism beneath the West Antarctic ice sheet and implications for ice-sheet stability. Nature 361, 526–529.

Blankenship, D.D., Bentley, C.R., Rooney, S.T., Alley, R.B., 1986. Seismic measurements reveal a saturated porous layer beneath an active Antarctic ice stream. Nature 322, 54–57.

Blankenship, D.D., Morse, D.L., Finn, C.A., Bell, R.E., Peters, M.E., Kempf, S.D., Hodge, S.M., Studinger, M., Behrendt, J.C., Brozena, J.M., 2001. Geologic controls on the initiation of rapid basal motion for West Antarctic ice streams: a geophysical perspective including new airborne radar sounding and laser altimetry results. In: Alley, R.B., Bindschadler, R.A. (Eds.), The West Antarctic Ice Sheet: Behavior and Environment. In: Antarct. Res. Ser., vol. 77. American Geophysical Union, Washington, DC, pp. 105–121.

Carter, S.P., Blankenship, D.D., Peters, M.E., Young, D.A., Holt, J.W., Morse, D.L., 2007. Radar-based subglacial lake classification in Antarctica. G-cubed 8.

Clarke, T.S., Burkholder, P.D., Smithson, S.B., Bentley, C.R., 1997. Optimum seismic shooting and recording parameters and a preliminary crustal model for the Byrd Subglacial Basin, Antarctica. In: Ricci, C.A. (Ed.), The Antarctic Region: Geological Processes and Evolution. Terra Antarctica, Siena, Italy, pp. 485–493.

Clow, G., Cuffey, K., Waddington, E., 2012. High heat-flow beneath the central portion of the West Antarctic ice sheet. In: AGU Fall Meeting Abstracts, p. 0577.

Corr, H.F.J., Vaughan, D.G., 2008. A recent volcanic eruption beneath the West Antarctic ice sheet. Nat. Geosci. 1, 122–125.

Dalziel, I.W.D., 2006. On the extent of the active West Antarctic rift system. Terra Antarct. 12, 193–202.

Dalziel, I.W.D., Elliot, D.H., 1982. West Antarctica: problem child of Gondwanaland. Tectonics 1, 3–19.

Dalziel, I.W.D., Lawver, L.A., 2001. The lithospheric setting of the West Antarctic ice sheet. In: Alley, R.B., Bindschadler, R.A. (Eds.), The West Antarctic Ice Sheet: Behavior and Environment. In: Antarct. Res. Ser., vol. 77. American Geophysical Union, Washington, DC, pp. 29–44.

Davies, J.H., 2013. Global map of solid Earth surface heat flow. Geochem. Geophys. Geosyst. 14, 4608–4622. http://dx.doi.org/10.1002/ggge.20271.

Diehl, T.M., 2008. Gravity analyses for the crustal structure and subglacial geology of West Antarctica, particularly beneath Thwaites Glacier. Dissertation. University of Texas at Austin.

Diehl, T.M. Holt, J.W. Blankenship, D.D. Young, D.A., 2008a. Free-air gravity anomalies over the Thwaites Glacier catchment, West Antarctica. Natl. Geophys. Data Cent., Boulder, CO.

Diehl, T.M., Holt, J.W., Blankenship, D.D., Young, D.A., Jordan, T.A., Ferraccioli, F., 2008b. First airborne gravity results over the Thwaites Glacier catchment, West Antarctica. Geochem. Geophys. Geosyst. 9, 251–256. http://dx.doi.org/10.1029/2007GC001878.

Eagles, G., Gohl, K., Larter, R.D., 2004. High-resolution animated tectonic reconstruction of the South Pacific and Western Antarctic margin. Geochem. Geophys. Geosyst. 5, 251–256. http://dx.doi.org/10.1029/2003GC000657.

Engelhardt, H., 2004. Ice temperature and high geothermal flux at Siple Dome, West Antarctica, from borehole measurements. J. Glaciol. 50, 251–256.

Fahnestock, M., Bamber, J., 2001. Morphology and surface characteristics of the West Antarctic ice sheet. In: Alley, R.B., Bindschadler, R.A. (Eds.), The West Antarctic Ice Sheet: Behavior and Environment. In: Antarct. Res. Ser., vol. 77. American Geophysical Union, Washington, DC, pp. 13–27.

Fairhead, J.D., Okereke, C.S., 1988. Depths to major density contrasts beneath the West African rift system in Nigeria and Cameroon based on the spectral analysis of gravity data. J. Afr. Earth Sci. 7, 769–777.

Ferraccioli, F., Jordan, T.A., Vaughan, D.G., Holt, J.W., James, M., Corr, H.F.J., Blankenship, D.D., Fairhead, J.D., Diehl, T.M., 2007. New aerogeophysical survey targets the extent of the West Antarctic Rift System over Ellsworth Land. In: Cooper, A.K., Raymond, C.R. (Eds.), Antarctica: A Keystone in a Changing World – Online Proceedings of the 10th ISAES X. USGS Open-File Report 2007-1047, Extended Abstract 113, Santa Barbara, California, pp. 1–4.

Fox Maule, C., Purucker, M.E., Olsen, N., Mosegaard, K., 2005. Heat flux in Antarctica revealed by satellite magnetic data. Science 309, 464–467. http://dx.doi.org/10.1126/science.1106888.

Fricker, H.A., Scambos, T., Carter, S., Davis, C., Haran, T., Joughin, I., 2010. Synthesizing multiple remote-sensing techniques for subglacial hydrologic mapping: application to a lake system beneath MacAyeal Ice Stream, West Antarctica. J. Glaciol. 56, 187–199.

Gohl, K., 2012. Basement control on past ice sheet dynamics in the Amundsen Sea Embayment, West Antarctica. Palaeogeogr. Palaeoclimatol. Palaeoecol. 335–336, 35–41. http://dx.doi.org/10.1016/j.palaeo.2011.02.022.

Gohl, K., Teterin, D., Eagles, G., Netzeband, G., Grobys, J.W.G., Parsiegla, N., Schlüter, P., Leinweber, V., Larter, R.D., Uenzelmann-Neben, G., Udintsev, G., 2007. Geophysical survey reveals tectonic structures in the Amundsen Sea embayment, West Antarctica. In: Cooper, A.K., Raymond, C.F. (Eds.), Antarctica: A Keystone in a Changing World – Online Proceedings of the 10th ISAES. Short Research Paper 047, USGS open-file report 2007-1047.

Holt, J.W., Blankenship, D.D., Morse, D.L., Young, D.A., Peters, M.E., Kempf, S.D., Richter, T.G., Vaughan, D.G., Corr, H.F.J., 2006. New boundary conditions for the West Antarctic ice sheet: subglacial topography of the Thwaites and Smith Glacier catchments. Geophys. Res. Lett. 33. http://dx.doi.org/10.1029/2005GL025561.

Huerta, A.D., Harry, D.L., 2007. The transition from diffuse to focused extension: modeled evolution of the West Antarctic Rift system. Earth Planet. Sci. Lett. 255 (1–2), 133–147. http://dx.doi.org/10.1016/j.epsl.2006.12.011.

Hwang, C.W., Hsiao, Y.S., Shih, H.C., Yang, M., Chen, K.H., Forsberg, R., Olesen, A.V., 2007. Geodetic and geophysical results from a Taiwan airborne gravity survey: data reduction and accuracy assessment. J. Geophys. Res. B, Solid Earth Planets 112 (B4). http://dx.doi.org/10.1029/2005jb004220.

Jachens, R.C., Griscom, J., 1985. An isostatic residual gravity map of California. In: Hinze (Ed.), The Utility of Regional Gravity and Magnetic Anomaly Maps. SEG Press, pp. 347–360.

Jacobs, S.A., Jenkins, A., Hellmer, H., Giulivi, C., Nitsche, F., Huber, B., Guerrero, R., 2012. The Amundsen Sea and the Antarctic Ice sheet. Oceanography 25 (3), 154–163. http://dx.doi.org/10.5670/oceanog2012.90.

Jankowski, E.J., Drewry, D.J., 1981. The structure of West Antarctica from geophysical studies. Nature 291, 17–21. http://dx.doi.org/10.1038/291017a0.

Jordan, T.A., Ferraccioli, F., Vaughan, D.G., Holt, J.W., Corr, H.F.J., Blankenship, D.D., Diehl, T.M., 2010. Aerogravity evidence for major crustal thinning under the Pine Island Glacier region (West Antarctica). GSA Bull. 122 (5–6), 714–726. http://dx.doi.org/10.1130/B26417.1.

Joughin, I., Smith, B.E., Medley, B., 2014. Marine ice sheet collapse potentially under way for the Thwaites Glacier Basin, West Antarctica. Science 344 (6185), 735–738.

Joughin, I., Tulaczyk, S., Bamber, J.L., Blankenship, D., Holt, J.W., Scambos, T., Vaughan, D.G., 2009. Basal conditions for Pine Island and Thwaites Glaciers, West Antarctica, determined using satellite and airborne data. J. Glaciol. 55, 245–257.

Kamb, B., 2001. Basal zone of the West Antarctic ice streams and its role in lubrication of their rapid motion. In: Alley, R.B., Bindschadler, R.A. (Eds.), The West Antarctic Ice Sheet: Behavior and Environment. In: Antarct. Res. Ser., vol. 77. American Geophysical Union, Washington, DC.

Karner, G.D., Watts, A.B., 1983. Gravity anomalies and flexure of the lithosphere at mountain ranges. J. Geophys. Res. 88, 10449–10477.

King, M.A., Bingham, R.J., Moore, P., Whitehouse, P.L., Bentley, M.J., Milne, G.A., 2012. Lower satellite-gravimetry estimates of Antarctic sea-level contribution. Nature 491, 586–589. http://dx.doi.org/10.1038/nature11621.

Lee, J., Shum, C.K., Howat, I.M., Monaghan, A., Ahn, Y., Duan, J., Guo, J.-Y., Kuo, C.-Y., Wang, L., 2012. Continuously accelerating ice loss over Amundsen Sea catchment, West Antarctica, revealed by integrating altimetry and GRACE data. Earth Planet. Sci. Lett. 321, 74–80. http://dx.doi.org/10.1016/j.epsl.2011.12.040.

LeMasurier, W.E., 2008. Neogene extension and basin deepening in the West Antarctic rift from comparisons with the East African rift and other analogs. Geology 36, 247–250.

LeMasurier, W.E., Landis, C.A., 1997. The West Antarctic erosional surface: its role in determining the timing of mantle plume activity, uplift, and erosion, during late cretaceous-cenozoic time in Marie Bird Land. In: Ricci, C.A. (Ed.), VII International Symposium on Antarctic Earth Sciences, The Antarctic Region; Geological Evolution and Processes. Terra Antarctica Publication, Siena, Italy, pp. 481–484.

LeMasurier, W.E., Thompson, J.W. (Eds.), 1990. Volcanoes of the Antarctic Plate and Southern Oceans. American Geophysical Union, Washington, DC. 487 pp.

Luyendyk, B.P., Sorlien, C.C., Wilson, D.S., Bartek, L.R., Siddoway, C.S., 2001. Structural and tectonic evolution of the Ross Sea rift in the Cape Colbeck region, Eastern Ross Sea, Antarctica. Tectonics 20, 933–958.

Luyendyk, B.P., Wilson, D.S., Siddoway, C.S., 2003. Eastern margin of the Ross Sea Rift in western Marie Byrd Land, Antarctica: crustal structure and tectonic development. Geochem. Geophys. Geosyst. 4. http://dx.doi.org/10.1029/2002GC000462.

McNutt, M.K., 1983. Influence of plate subduction on isostatic compensation in Northern California. Tectonics 2, 399–415.

Olesen, A., 2002. Improved airborne scalar gravimetry for regional gravity field mapping and geoid determination. Dissertation thesis. University of Copenhagen, Denmark. 50 pp.

Palais, J.M., Kyle, P.R., McIntosh, W.C., Seward, D., 1988. Magmatic and Phreatomagmatic volcanic activity at Mt Takahe, West Antarctica, based on Tephra Layers in the Byrd Ice Core and Field Observations at Mt Takahe. J. Volcanol. Geotherm. Res. 35, 295–317.

Peters, L.E., Anandakrishnan, S., Alley, R.B., Smith, A.M., 2007a. Extensive storage of basal meltwater in the onset region of a major West Antarctic ice stream. Geology 35, 251–254.

Peters, M.E., Blankenship, D.D., Carter, S.P., Kempf, S.D., Young, D.A., Holt, J.W., 2007b. Along-track focusing of airborne radar sounding data from West Antarctica for improving basal reflection analysis and layer detection. IEEE Trans. Geosci. Remote Sens. 45, 2725–2736.

Pollack, H.N., Hurter, S.J., Johnson, J.R., 1993. Heat flow from the Earth's interior: analysis of the global data set. Rev. Geophys. 31, 267–280.

Pritchard, H.D., Arthern, R.J., Vaughan, D.G., Edwards, L.A., 2009. Extensive dynamic thinning on the margins of the Greenland and Antarctic ice sheets. Nature 461, 971–975.

Regan, R.D., Hinze, W.J., 1976. The effect of finite data length in the spectral analysis of ideal gravity anomalies. Geophysics 41, 44–55.

Rignot, E., 2006. Changes in ice dynamics and mass balance of the Antarctic ice sheet. Philos. Trans. R. Soc., Math. Phys. Eng. Sci. 364, 1637–1655.

Rignot, E., Jacobs, S., Mouginot, J., Scheuchl, B., 2013. Ice-shelf melting around Antarctica. Science 341, 266–270. http://dx.doi.org/10.1126/science.1235798.

Rignot, E., Mouginot, J., Morlighem, M., Seroussi, H., Scheuchl, B., 2014. Widespread, rapid grounding line retreat of Pine Island, Thwaites, Smith, and Kohler glaciers, West Antarctica, from 1992 to 201. Geophys. Res. Lett. 41, 3502–3509.

Risk, G.F., Hochstein, M.P., 1974. Heat flow at arrival heights, Ross Island, Antarctica. N.Z. J. Geol. Geophys. 17, 629–644.

Ritzwoller, M.H., Shapiro, N.M., 2003. Crustal and upper mantle structure beneath Antarctica and surrounding oceans. In: Open File Report, REVEAL: Remote Views and Exploration of Antarctic Lithosphere Workshop: The Future of Antarctic Airborne Geophysical Capabilities – Workshop Report. United States Geological Survey, Washington, DC. 99 pp.

Ritzwoller, M.H., Shapiro, N.M., Levshin, A.L., Leahy, G.M., 2001. Crustal and upper mantle structure beneath Antarctica and surrounding oceans. J. Geophys. Res. B, Solid Earth Planets 106, 30645–30670.

SCAR – The Scientific Committee on Antarctic Research, 2006. Antarctic Digital Database (ADD). Accessed 2008. Online: http://www.add.scar.org:8080/add/.

Schroeder, D.M., Blankenship, D.D., Young, D.A., Quartini, E., 2014. Evidence for elevated and spatially variable geothermal flux beneath the West Antarctic Ice Sheet. Proc. Nat. Acad. Sci. USA 111, 9070–9072. http://dx.doi.org/10.1073/pnas.1405184111.

Sergienko, O.V., Hindmarsh, R.C.A., 2013. Regular patterns in frictional resistance of ice-stream beds seen by surface data inversion. Science 342, 1086–1089. http://dx.doi.org/10.1126/science.1243903.

Shapiro, N.M., Ritzwoller, M.H., 2004. Inferring surface heat flux distributions guided by a global seismic model: particular application to Antarctica. Earth Planet. Sci. Lett. 223, 213–224.

Shepherd, A., 45 others, 2012. A reconciled estimate of ice-sheet mass balance. Science 338 (6111), 1183–1189. http://dx.doi.org/10.1126/science.1228102.

Siddoway, C.S., 2008. Tectonics of the West Antarctic Rift System: new light on the history and dynamics of distributed intracontinental extension. In: Cooper, A.K., Barrett, P.J., Stagg, H., Storey, B., Stump, E., Wise, W., t.t.l.e. team (Eds.), Antarctica: A Keystone in a Changing World. Proceedings of the 10th International Symposium on Antarctic Earth Sciences. The National Academies Press, Washington, DC.

Siegert, M.J., Carter, S., Tabacco, I., Popov, S., Blankenship, D.D., 2005. A revised inventory of Antarctic subglacial lakes. Antarct. Sci. 17, 453–460.

Sieminski, A., Debayle, E., Lévêque, J.-J., 2003. Seismic evidence for deep low-velocity anomalies in the transition zone beneath West Antarctica. Earth Planet. Sci. Lett. 216, 645–661.

Smith, D.A., Holmes, S.A., Li, X., Guillaume, S., Wang, Y.M., Burki, B., Roman, D.R., Damiani, T.M., 2013. Confirming regional 1 cm differential geoid accuracy from airborne gravimetry: the Geoid Slope Validation Survey of 2011. J. Geodes. 87, 885–907. http://dx.doi.org/10.1007/s00190-013-0653-0.

Spector, A., Grant, F.S., 1970. Statistical models for interpreting aeromagnetic data. Geophysics 35, 293–302.

Studinger, M., Bell, R.E., Blankenship, D.D., Finn, C.A., Arko, R.A., Morse, D.L., Joughin, I., 2001. Subglacial sediments: a regional geological template for ice flow in West Antarctica. Geophys. Res. Lett. 28. http://dx.doi.org/10.1029/2000GL011788.

Talwani, M., Worzel, J.L., Landisman, M., 1959. Rapid gravity computations for two-dimensional bodies with application to the Mendocino submarine fracture zone. J. Geophys. Res. 64 (1), 29–59. http://dx.doi.org/10.1029/JZ064i001p00049.

Tapley, B., Ries, J., Bettadpur, S., Chambers, D., Cheng, M., Condi, F., Poole, S., 2007. The GGM03 mean earth gravity model from GRACE. Eos Trans. AGU 88 (52). Fall Meet. Suppl., Abstract G42A-03.

Thomas, R., Rignot, E., Casassa, G., Kanagaratnam, P., Acuña, C., Akins, T., Brecher, H., Frederick, E., Gogineni, P., Krabill, W., Manizade, S., Ramamoorthy, H., Rivera, A., Russell, R., Sonntag, J., Swift, R., Yungel, J., Zwally, J., 2004. Accelerated sea-level rise from West Antarctica. Science 306. http://dx.doi.org/10.1126/science.1099650.

Tinto, K.J., Bell, R.E., 2011. Progressive unpinning of Thwaites Glacier from newly identified offshore ridge: constraints from aerogravity. Geophys. Res. Lett. 38 (20). http://dx.doi.org/10.1029/2011GL049026.

Vaughan, D.G., Bamber, J., Giovinetto, M., Russell, J., Cooper, A.P.R., 1999. Reassessment of net surface mass balance in Antarctica. J. Clim. 12, 933–946.

Vaughan, D.G., Corr, H.F.J., Ferraccioli, F.F., Frearson, N., O'Hare, A., Mach, D., Holt, J.W., Blankenship, D.D., Morse, D.L., Young, D.A., 2006. New boundary conditions for the West Antarctic ice sheet: subglacial topography beneath Pine Island Glacier. Geophys. Res. Lett. 33. http://dx.doi.org/10.1029/2005GL025588.

Vaughan, D.G., Holt, J.W., Blankenship, D.D., 2007. West Antarctic links to sea level estimation. Eos Trans. AGU 88. http://dx.doi.org/10.1029/2007EO460001.

Vogel, S.W., Tulaczyk, S., 2006. Ice-dynamical constraints on the existence and impact of subglacial volcanism on West Antarctic ice sheet stability. Geophys. Res. Lett. 33.

von Frese, R.R.B., Hinze, W.J., Braile, L.W., Luca, A.J., 1981. Spherical earth gravity and magnetic anomaly modeling by Gauss–Legendre quadrature integration. J. Geophys. 49, 234–242.

Wannamaker, P.E., Stodt, J.A., Olsen, S.L., 1996. Dormant state of rifting below the byrd subglacial basin, West Antarctica, implied by magnetotellurgic (MT), profiling. Geophys. Res. Lett. 23, 2983–2986.

Wessel, P., Smith, W.H.F., 1998. New, improved version of Generic Mapping Tools released. Eos Trans. AGU 79 (47), 579.

Winberry, J.P., Anandakrishnan, S., 2004. Crustal structure of the West Antarctic rift system and Marie Bird Land hotspot. Geology 32, 977–980.

Young, D.A., Kempf, S.D., Blankenship, D.D., Holt, J.W., Morse, D.L., 2008. New airborne laser altimetry over the Thwaites Glacier Catchment, West Antarctica. G-cubed 9.